Water Supply

Water Supply Vol 22 No 4, 3993 doi: 10.2166/ws.2022.029

Ozone water production using a SPE electrolyzer equipped with boron doped diamond electrodes

H. Y. Li, C. Deng*, L. Zhao, C. H. Gong, M. F. Zhu and J. W. Chen

Institute of Medical Support Technology, Academy of System Engineering, Academy of Military Sciences, NO.106 Wangdong Road, Hedong District, Tianjin 300161, China
*Corresponding author. E-mail: dcnudt@163.com

ABSTRACT

Electrochemical ozone production (EOP) is an attractive technology for disinfection and sterilization purposes. This work reports a study on the EOP performance of the solid polymer electrolyte (SPE) electrolyzer, including the optimization of electrode configuration and operation conditions. It is proven that the EOP performance is highly affected by electrode configuration. Tests using BDDs with different B/C ratios demonstrate that BDD-4.9 provides more reaction sites and faster electron transfer rate, exhibiting a high electrocatalytic activity for EOP. Regarding electrode thickness, 0.54 mm in thickness is the most suitable for the EOP from the perspective of less power consumption. Moreover, operation conditions were evaluated. It was found that increasing water flow rate is an effective strategy for promoting ozone dissolution, and within the present experimental range, the water flow rate of 63 $L{\cdot}h^{-1}$ was identified. Meanwhile, through the study of all processes occurring inside the electrolyzer at higher current densities, the optimum current density was determined to be 125 $mA{\cdot}cm^{-2}$. Based on these results, ozone water presents excellent performance in the killing of *Escherichia coli* with high inoculum concentrations, indicating potential application performance in the field of environment.

Key words: bactericidal capability, boron-doped diamond, membrane electrode assembly, ozone water, solid polymer electrolyte

HIGHLIGHTS

- Ozone production by electrochemical technology.
- The SPE electrolyzer with specially designed clamping system served as the ozone reactor.
- Using a boron-doped diamond (BDD) as the electrode material.
- The SPE electrolyzer can continuously and effectively produce ozone by a flow-through system with low energy consumption.
- Ozone water shows a considerable bactericidal effect on different concentrations of *E. coli*.

GRAPHICAL ABSTRACT

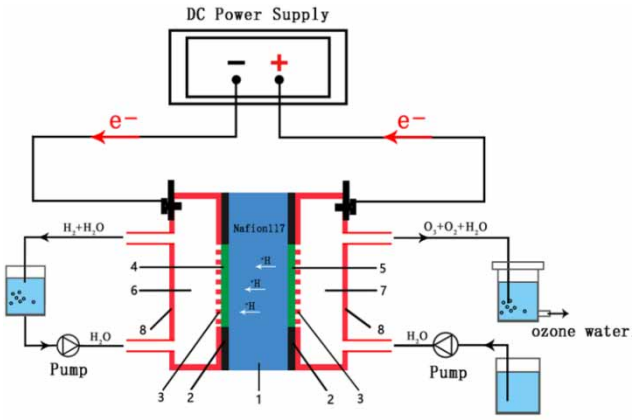

1.Nafion117, 2.Gasket, 3.Fluid manifold, 4.Cathode(BDD), 5.Anode(BDD),
6.Cathode compartment, 7.Anode compartment, 8.Titanium current collector

INTRODUCTION

Ozone, with a high oxidation potential of 2.076 V (vs RHE) (Ershov & Morozov 2008), can rapidly and efficiently remove a large variety of contaminants and pathogens (Rosal *et al.* 2008; García-Espinoza *et al.* 2021) and is widely used in the fields of sterilization, disinfection, and water treatment(Uhm *et al.* 2009; Goztas *et al.* 2014; Lara-Ramos *et al.* 2020). Meanwhile, ozone is very environmentally friendly compared with many other oxidants such as chlorine because it is unstable and spontaneously decomposes into oxygen, leaving no harmful residuals during its application (Awad *et al.* 2006a). Due to these properties, intensive interest has been generated in efficient methods of ozone production.

Conventional technologies for generating ozone have been developed including corona discharge and ultraviolet radiation (Azam *et al.* 2019; Rodríguez-Peña *et al.* 2021c). However, these two methods cannot satisfy the application requirements in some aspects owing to their inherent limitations. For instance, the corona discharge not only requires very high voltages and additional equipment but also releases harmful nitrogen oxides (Lees *et al.* 2018). Ultraviolet radiation shows high energy consumption. In addition, both methods can only produce ozone gas, which is limited to space environment disinfection. Electrochemical technology casts a light on ozone production, which can directly produce a high concentration of ozone water at low voltages, thereby skipping the problems associated with dissolving ozone gas into water (Zhang *et al.* 2017; Sandin *et al.* 2020). Therefore, this technology is available for substance surface disinfection such as the hands and food as well as surgical equipment washing. The structure of the electrolyzer is crucial to the actual application of this technology.

At present, the solid polymer electrolyte (SPE) electrolyzer is regarded as a more rational design to generate ozone water than with the separated electrolyzer. In a SPE electrolyzer, the following reactions (equations 1–3) occur at the anode and cathode.

$$\text{anode reactions} \quad 3H_2O \rightarrow O_3 + 6H^+ + 6e^- \quad E_0 = +1.5 \text{ V (vs RHE)} \tag{1}$$

$$2H_2O \rightarrow O_2 + 4H^+ + 4e^- \quad E_0 = +1.23 \text{ V (vs RHE)} \tag{2}$$

$$\text{cathode reactions} \quad 2H^+ + 2e^- \rightarrow H_2 \quad E_0 = 0.0 \text{ V (vs RHE)} \tag{3}$$

It is noteworthy that the formation of O_3 by oxidation of water (see equation (1)) is in strong competition with oxygen evolution (see equation (2)), which is thermodynamically preferred at a lower redox potential (Santana *et al.* 2005). In addition, the electrodes suffer from corrosion and passivation due to the harsh environment that is induced by the formation of hydrogen ions at the anode interface. Thus, electrode materials play a prominent role in ozone production. Firstly, the anode materials need high overvoltage for the oxygen evolution reaction (OER) to encourage the generation of O_3 and retard the evolution of O_2, resulting in the high current efficiencies. Secondly, the anode materials should have good chemical and thermal stability to resist chemical corrosion.

In previous studies various electrode materials, especially PbO_2 (Wang *et al.* 2008; Wang & Jing 2012), Pt (Awad *et al.* 2006b), and glassy carbon (Foller & Kelsall 1993), have been thoroughly investigated and show remarkable performance for ozone production. Nevertheless, they still have some drawbacks, such as electrode erosion caused by oxidation reactions and considerably extreme conditions required (Rodríguez-Peña *et al.* 2021b). As an emerging potential candidate, boron-doped diamond (BDD) meets the abovementioned requirements well, and its inert surface with weak adsorption properties endows the ability to permit the stable presence of OH· and O·, which act as precursors for ozone production. Moreover, it shows excellent electrical conductivity (Mortet & Soltani 2011), a wide electrochemical window (Zhang *et al.* 2021), and high electrocatalytic activity, which could improve the mass transfer process and reach higher energy efficiencies.

However, several studies revealed that BDD electrode had relatively low electrochemical ozone production (EOP) performance as a result of high cell voltage. The composition and structure of BDD have been demonstrated to be key to solving the problem. Arihara *et al.* (2007) prepared a BDD electrode by optimizing the number of holes, hole size, and electrode thickness, achieving a maximum current efficiency of 47%. Honda *et al.* (2013) compared BDD electrodes with various B/C ratios using an electrolyte-free system and it was found that heavily BDD electrodes with sp^2 impurities yielded a high concentration of ozone.

In addition, operation conditions are also very important for the EOP performance. Kraft *et al.* (2006) utilized BDDs as cathode and anode, investigating the effects of current density, flow rate, and electrolyte conductivity on ozone production in a SPE electrolyzer, and it was found that high flow rate and low conductivity of water are beneficial to ozone production. Rodríguez-Peña *et al.* (2021a) proposed a phenomenological model to explain the influence of the current intensity applied, helping to understand the basis of the electrochemical processes that occur inside the cell and promote the production of ozone.

In summary, the further advance of the EOP performance can be improved by optimizing electrode configuration and operating conditions simultaneously. Herein, based on SPE technology, we conducted the structural design of the ozone reactor, in which BDDs were employed as electrode materials to research the performance of ozone production. The influence of electrode configuration and operation conditions on ozone generation performance were systematically investigated. Finally, the bactericidal activity of ozone water is evaluated. This study provides technical support for the large-scale application of the EOP technology.

MATERIALS AND METHODS

Materials and reagents

All of the chemical reagents were directly used without treatment. Indigo carmine ($C_{16}H_8N_2Na_2O_8S_2$), potassium dihydrogen phosphate (KH_2PO_4), dibasic sodium phosphate (Na_2HPO_4), sulfuric acid (H_2SO_4, 98%), hydrogen peroxide (H_2O_2), tryptone, sodium chloride (NaCl), bovine serum albumin (BSA), nutrient broth (NB), agar, and sodium thiosulfate ($Na_2S_2O_3$) were purchased from Tianjin Kemiou Chemical Reagent Co., Ltd. *Escherichia coli* (8099) was supplied by the National Bio-Protection Engineering Center of China. Nafion 117 (Dupont, 50 mm × 50 mm) as a SPE membrane was obtained from Shanghai Fanyue Electronic Technology Co., Ltd. BDDs employed as electrodes (40 mm × 40 mm) were bought from by Luoyang Yuxin Diamond Co., Ltd. Deionized water used to prepare all the solutions was produced by the Millipore Milli-Q system (conductivity: 1 $\mu s \cdot cm^{-1}$).

Experimental setup

As illustrated in Figure 1, there is a Nafion 117 membrane between two BDD electrodes, gaskets outside the electrodes, titanium current collectors outside the gaskets. The gaskets were adequately compressed through a specially designed clamping system, so that BDD electrodes were firmly attached to both sides of the Nafion 117 membrane. This compact structure helps not only reduce ohmic loss, but also prevent gas-liquid channeling and water leakage. Fluid manifolds that are machined into titanium plates ensure uniform distribution of water in the electrolyzer and provide the necessary conditions for full contact between BDD electrodes and water. Additionally, it can export the gas and heat generated in time to reduce the resistance loss of the flow channels. Titanium as a current collector has the function of providing a conductor for the transfer of charges.

As described in Figure 2, the electrolyzer was powered by a DC power supply (M8811, Maynuo, China). Deionized water was continuously fed into both anode and cathode compartments using two peristaltic pumps (BT100S-1, LEAD FLUID, China) at different flow rates (9, 18, 27, 36, 45, 54, 63, 72, and 81 $L \cdot h^{-1}$). Water is oxidized to ozone and oxygen at the anode surface. Hydrogen ions in hydrated form move through the membrane to the cathode. Meanwhile, electrons reach

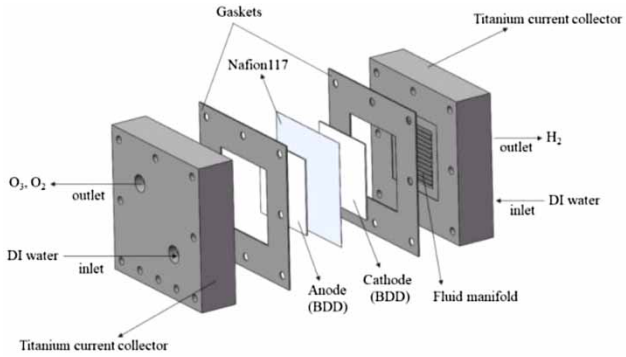

Figure 1 | Structure of the SPE electrolyzer.

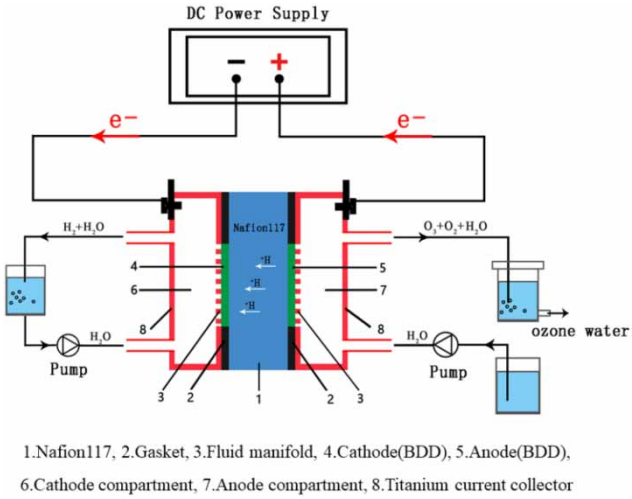

Figure 2 | Scheme of the experimental setup for electrochemical ozone water production.

the cathode through the external circuit. Finally, they meet at the cathode surface and the reduction reaction occurs to evolve hydrogen. The experiments were performed under galvanostatic conditions (0.5, 1, 1.5, 2, 2.5, 3, 3.5, 4, 4.5, and 5 A).

Analytical techniques

Measurement of ozone concentration

The concentration of ozone water was determined by indigo disulfonate spectrophotometry (IDS). The photometric measurements were performed in a UV-VIS spectrophotometer (Hach, Model: DR5000).

Assessment of ozone production performance

The EOP performance was evaluated by current efficiency and specific power consumption.

The proportion of electric current that is used to produce ozone is defined as current efficiency, and is calculated by Equation (4):

$$current\ efficiency\ (\%) = \frac{n\,F\,V_w\,C_{O_3}}{3600\,M\,I} \tag{4}$$

where n is the stoichiometric number of electrons transferred, F is the Faraday's constant (9.6485×10^4 C·mol^{-1}), V_w is the water flow rate (L·h^{-1}), C_{O_3} is the concentration of ozone water (g·L^{-1}), M is the molecular weight of ozone (48 g·mol^{-1}), and I is the current (A).

Specific power consumption is the energy consumed to produce one gram of ozone, and is calculated by Equation (5):

$$specific\ power\ consumption\ (Wh \cdot g^{-1}) = \frac{I\ U}{V_w C_{o_3}} \tag{5}$$

where U is corresponded to cell voltage (V).

Composition and structure characterization

The composition and morphology of the BDD electrodes were characterized by a scanning electron microscope (SEM, Sigma 300, Zeiss, Germany) combined with energy dispersive X-ray spectrometry (EDS, Smart EDX, Zeiss, Germany). The crystal structure of the BDD electrode was analyzed by X-ray diffraction (XRD, Ultima IV, Rigaku, Japan) with Cu-Kα radiation (λ = 1.5418 nm) at a scanning rate of 2° min^{-1}. The crystal quality of the BDD electrode was examined by a Raman spectrometer (LabRAM HR Evolution, HORIBA Scientific, France) with a 532 nm laser.

Evaluation of the bactericidal performance of ozone water

Preparation of *E. coli* suspension: prior to the experiments, the *E. coli* seed tube was thawed and sub-cultured for 18–24 h at 37 °C on nutrient agar (NA) (Graça *et al.* 2011). After NA growth, at least three well-isolated colonies were selected and transferred with an inoculation loop into a tube containing 10 mL of nutrient broth and then was cultivated in a constant temperature incubator (MCo-175, SANYO, Japan) for 18–24 h at 37 °C. The initial prepared *E. coli* suspension was diluted to the required concentrations and maintained in a refrigerator at 4 °C for later use.

Suspension quantitative sterilization test: a mixture of 0.5 mL of the *E. coli* suspension and 0.5 mL of organic interference (3% BSA) was exposed to 4.0 mL of ozone water for 2 min, followed by taking 0.5 mL of sample and adding it to 4.5 mL of a neutralizer (PBS, 0.03 mol·L^{-1}, pH 7.2, with 10 g·L^{-1} sodium thiosulfate) (Santos *et al.* 2021). After the exposed time of 10 min, the sample was inoculated in triplicate in plate count agar (PCA) for 18–24 h at 37 °C. A positive control repeated the above operation using tryptone saline solution (TPS) instead of ozone water.

The death rate of *E. coli* is calculated using the mean colony counts of three agar plates according to Equation (6):

$$Death\ rate\ (\%) = \frac{N_0 - N_x}{N_0} \tag{6}$$

where N_0 is the colony count of the positive control (cfu·mL^{-1}), N_x is the colony count of the test (cfu·mL^{-1}).

Additionally, growth reduction of *E. coli* is calculated according to Equation (7):

$$Growth\ reduction\ =\ log_{10}(N_0)\ -\ log_{10}(N_x) \tag{7}$$

RESULTS AND DISCUSSION

Characterization of the BDD electrodes

As shown in Figure 3(b) and 3(c) elements distribute on the surface of BDD electrodes uniformly, indicating the well incorporation of boron atoms into the diamond structure. The carbon content of three BDD electrodes is determined to be 98.95 wt%, 97.45 wt%, and 95.33 wt%, respectively, and the boron content is determined to be 1.05 wt%, 2.55 wt%, and 4.9 wt%, respectively. Therefore, the weight ratios of boron and carbon (B/C ratios) of the three BDD electrodes are 1.1%, 2.6%, 4.9%, which are denoted as BDD-1.1, BDD-2.6 and BDD-4.9, respectively.

Observing the morphology of the BDD electrodes by SEM, as shown in Figure 4. The grain size of BDD electrodes is varied from 11 to 87 μm. And the array of BDD electrodes is continuous and uniform, and their grains are smooth and sharp, proving they have good crystallinity as well as no obvious cracks. The tightly arranged structure of the BDD electrodes shows strong resistance to oxidation and corrosion, which is beneficial to prevent the penetration of electrolyte and improve the stability of the electrode.

XRD was used to further investigate the crystal structures of BDD electrodes, as shown in Figure 5(a). For three BDD electrodes, the characteristic diffraction peaks of diamond are clearly observed at 43.94°, 75.22°, and 91.42°, which are assigned for the (111), (220), and (311) planes of the diamond. The diamond (220) is the dominant growth direction in the BDD-1.1

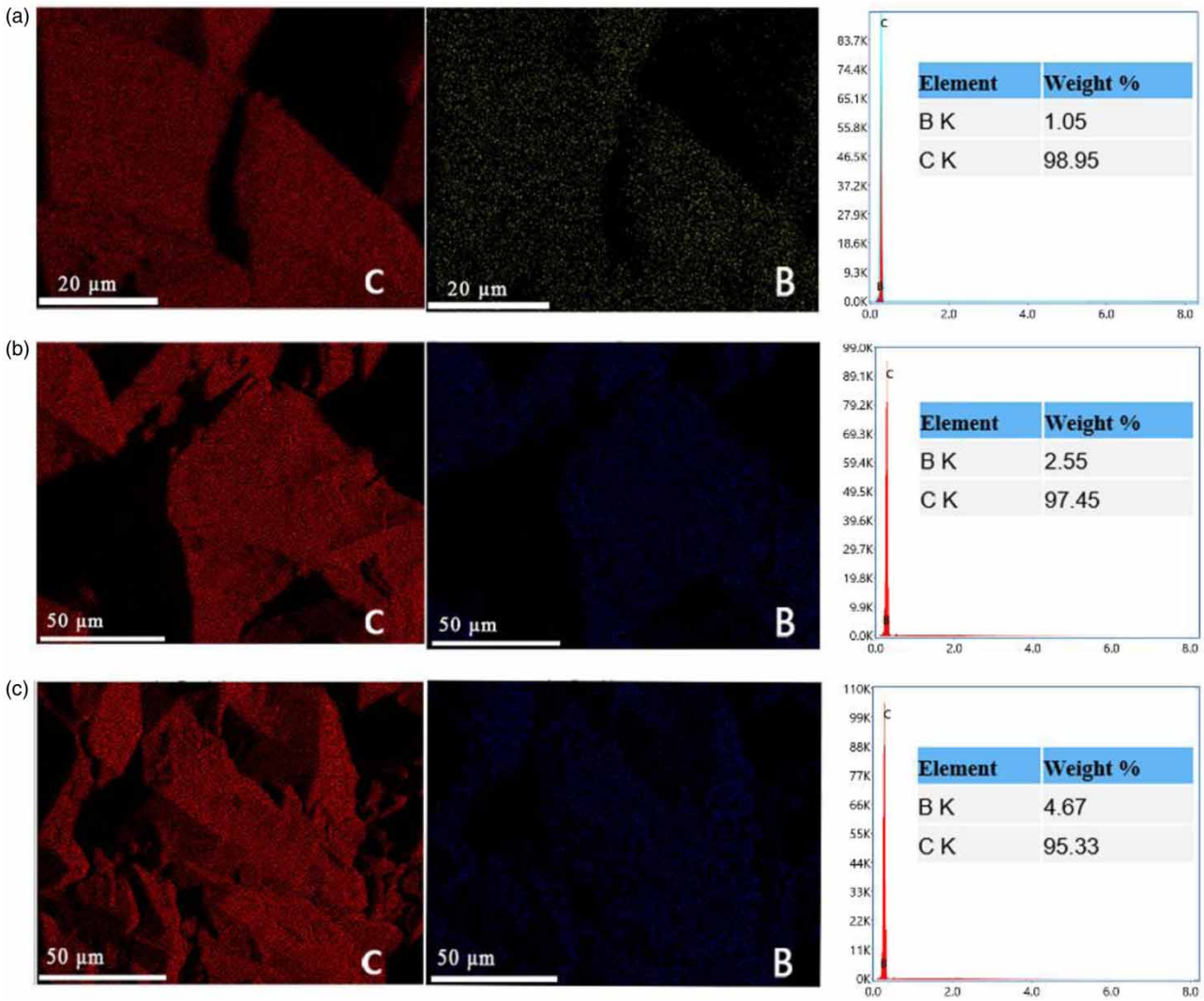

Figure 3 | (a–c) EDS results and elemental mapping images of three BDD electrodes.

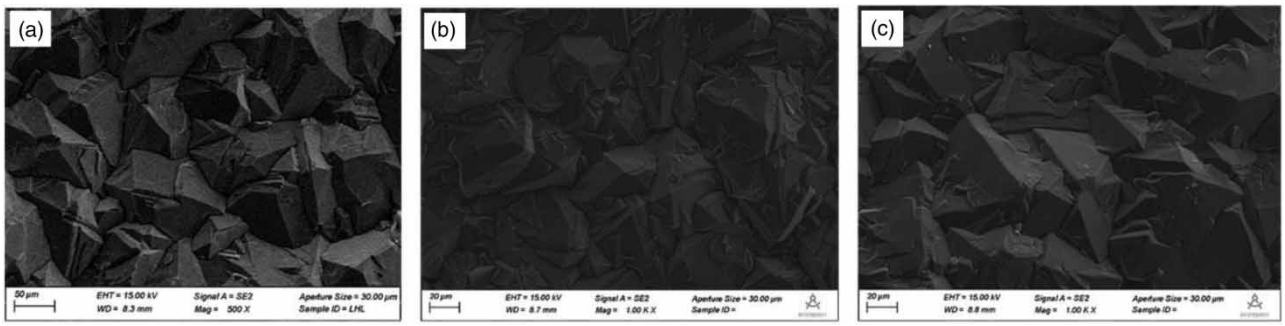

Figure 4 | SEM images of (a) BDD-1.1, (b) BDD-2.6, and (c) BDD-4.9 electrodes.

electrode and the diamond (111) is the dominant growth direction in both of BDD-2.6 and BDD-4.9 electrodes. And the (111) plane of the BDD-4.9 electrode is more intense than BDD-2.6. This observation confirms that the (111) plane promotes the incorporation of boron atoms the most and has a crucial impact on the electrical and electrochemical properties such as conductivity and active surface area.

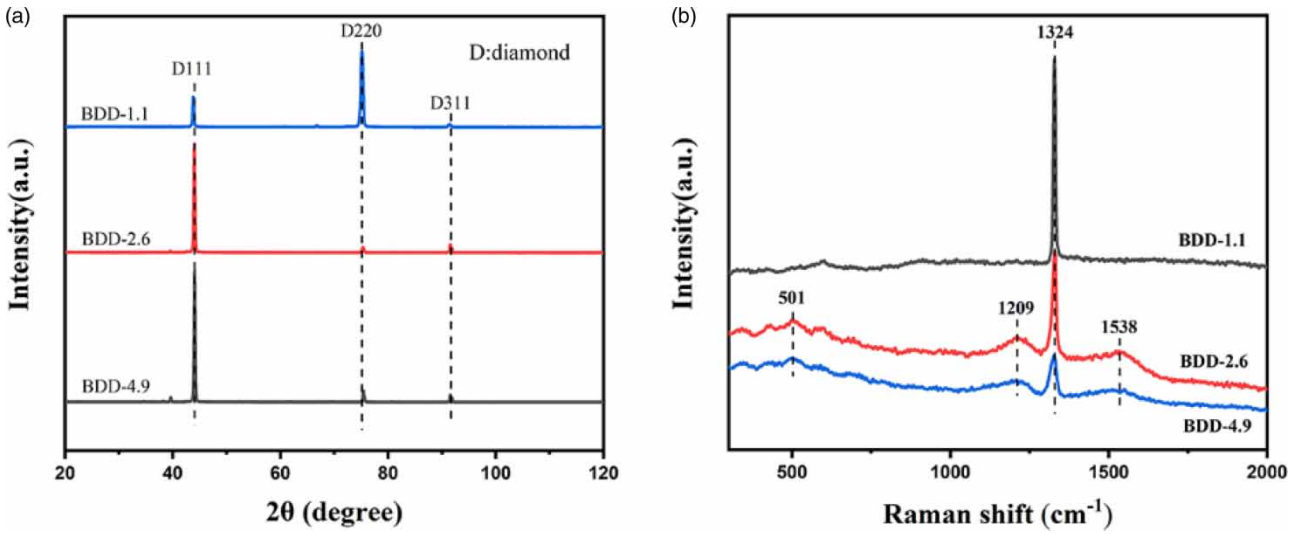

Figure 5 | (a) XRD patterns and (b) Raman spectra of BDD-1.1, BDD-2.6, and BDD-4.9 electrodes.

The Raman spectra of the BDD electrodes were taken to determine their crystal quality (Figure 5(b)). For three BDD electrodes, the characteristic peak at 1,324 cm^{-1} corresponds to the diamond having a significant negative shift compared to the standard diamond peak (1,324 cm^{-1}), which can be attributed to nonideal crystal form appearing in the diamond. Two typical broadband peaks of BDD-2.6 and BDD-4.9 electrodes can be observed at 501 and 1,209 cm^{-1}, which are attributed to the heavily doping of boron (Okino *et al.* 2004). Besides, the spectrums of BDD-2.6 and BDD-4.9 electrodes also display a typical broadband peak at 1,538 cm^{-1}, which is induced by the G (graphite carbon) bands (Coffinier *et al.* 2011). Notably BDD-2.6 and BDD-4.9 electrodes only have a low amount of graphite carbon, confirming almost no lattice defects in BDD electrodes (Zhao *et al.* 2014).

The changes in EOP performance with B/C ratio

To explore the effect of the boron doping amount on the EOP performance, the three BDD electrodes under different current densities were tested at an electrode thickness of 0.32 mm and a flow rate of 36 $L{\cdot}h^{-1}$ (Figure 6).

Figure 6(a) demonstrates that the ozone concentration produced by the three BDD electrodes is virtually identical when the current density is lower than 125 $mA{\cdot}cm^{-2}$. On the contrary, accompanied with increasing current density, BDD-4.9 electrode shows higher ozone concentration and it is up to 7.686 $mg{\cdot}L^{-1}$ at the current density of 312.5 $mA{\cdot}cm^{-2}$. The result verifies that a BDD electrode with a high B/C ratio can promote formation of dissolved O_3.

As shown in Figure 6(b), the cell voltage increases with the current density, and at each given current density, the value of BDD-4.9 electrode is significantly lower than those of BDD-1.1 and BDD-2.6 electrodes. Moreover, it can also be seen from the slope of the curve, the higher the B/C ratio, the slower the rising rate of cell voltage. Those results indicate that increasing the boron doping amount is an effective strategy to lower cell voltage under the condition of keeping high BDD quality, which is because that the enhanced boron doping can reduce resistance and yield higher conductivity (Liu *et al.* 2011).

As observed in Figure 6(c), the initial current efficiency increases with increasing current density regardless of the studied B/C ratio. After reaching a maximum value at 125 $mA{\cdot}cm^{-2}$, the current efficiency decreases with increasing current density. This result confirms a medium current density is more conducive to produce O_3. At the case of current density below 125 $mA{\cdot}cm^{-2}$, the reason for the increase of current efficiency is that the OER process is gradually replaced by the EOP process with increasing current density. At the case of current density over 125 $mA{\cdot}cm^{-2}$, a decrease in the current efficiency may be a result of the following factors: firstly, the anodic oxidation of water to produce hydrogen peroxide competes with the production of ozone, as described in Equation (8):

$$2H_2O \rightarrow H_2O_2 + 6H^+ + 6e^- \quad (8)$$

Secondly, hydrogen peroxide as a predator of ozone can interact with ozone and destroy it, as shown in Equation (9):

$$O_3 + H_2O_2 \rightarrow 2O_2 + H_2O \quad (9)$$

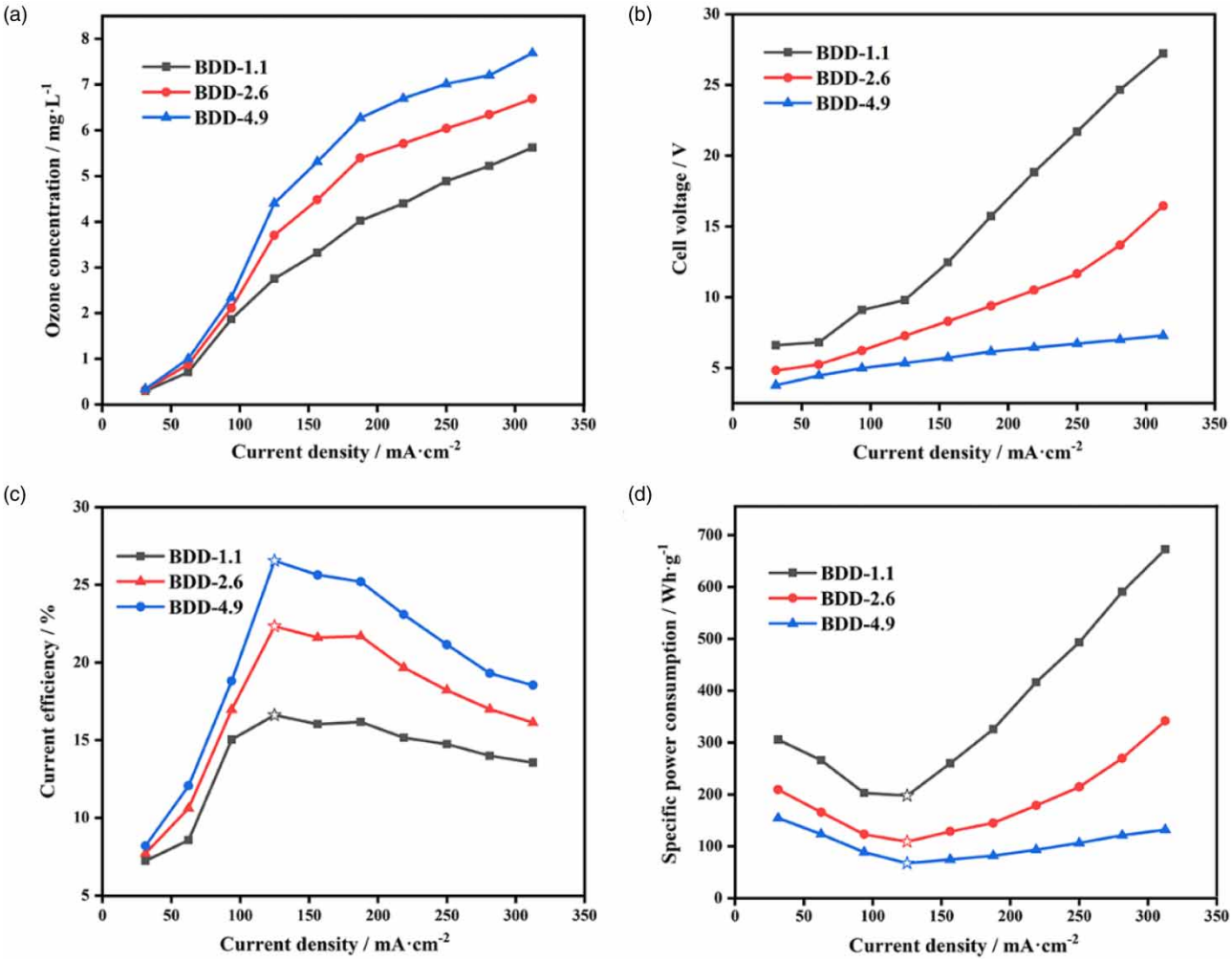

Figure 6 | The dependence of (a) ozone concentration, (b) cell voltage, (c) current efficiency, (d) specific power consumption on current density using BDD-1.1, BDD-2.6 and BDD-4.9 electrodes.

It has to be highlighted the kinetics of Equation (9) depends on the concentration of H_2O_2. Higher current density leads to an increase in the concentration of H_2O_2, enhancing the kinetics in Equation (9) and accelerating ozone destruction (Michaud *et al.* 2003). Meanwhile, increasing current density increases the heat generated on the three-phase interface that is a contact surface formed among the BDD electrodes, Nafion 117, and water. This phenomenon leads to a rise in temperature, which accelerates the chemical decomposition of ozone and reduces the current efficiency. The three factors mentioned above affect negatively the accumulation of ozone, causing a decay in the current efficiency.

It can also be seen from Figure 6(c), the BDD-4.9 electrode has the higher current efficiency than BDD-1.1 and BDD-2.6 electrodes under different current densities, and it reaches 26.6% when the current density is 125 mA·cm-2. This trend can be explained by the mechanism of ozone generation (Equations (10–13)) proposed by Babak *et al.* (1994) and Da Silva *et al.* (2003), (Silva *et al.* 2001)

$$H_2O \rightarrow (OH\cdot)_{ads} + H^+ + e^- \quad (10)$$

$$(OH\cdot)_{ads} \rightarrow (O\cdot)_{ads} + H^+ + e^- \quad (11)$$

$$2(O\cdot)_{ads} \rightarrow (O_2)_{ads} \rightarrow O_2 \quad (12)$$

$$(O\cdot)_{ads} + (O_2)_{ads} \rightarrow (O_3)_{ads} \rightarrow O_3 \quad (13)$$

According to the mechanism, the terminal O_3 generation depends on Equation (13), and increasing the coverage of the key intermediates of O_2^* and O* on the surface of the active centers increases their encounter chances, thereby accelerating the EOP kinetics. Hydroxyl radical intermediates are the precursor of oxygen intermediates. BDD with a high B/C ratio exhibits a larger active surface area, which can provide more reaction sites to promote the absorption of hydroxyl radical, thus increasing concentrations of oxygen intermediates on electrode surface (Gu *et al.* 2021). Therefore, a higher current efficiency was achieved when using the BDD-4.9 electrode. Besides, the BDD electrode with a high B/C ratio shows a higher carrier concentration, which accelerates electron transfer rate (Bogdanowicz *et al.* 2020; Dettlaff *et al.* 2020), and a faster electron transfer rate can enhance the terminal rate of O_3 generation, thus improving current efficiency. Based on the results represented above, we conclude that increasing B/C ratio of BDD electrodes is a feasible strategy to improve ozone production rate, and the BDD electrode with a high B/C ratio shows a high electrocatalytic activity for EOP.

Figure 6(d) displays that regardless of the studied B/C ratio, the specific power consumption with current density first decreases down to a minimum value, and then increases. The specific power consumption decreases depending on the boron doping level in the order of BDD-1.1, BDD-2.6, and BDD-4.9. The minimum value of 67.44 $Wh \cdot g^{-1}$ is obtained by BDD-4.9 electrode at a current density of 125 $mA \cdot cm^{-2}$, indicating that the BDD electrode with a high B/C ratio has remarkable EOP performance.

The changes in EOP performance with BDD electrode thickness

To investigate the influence of electrode thickness on the EOP performance, BDD electrodes with different thicknesses in the range of 0.32–0.98 mm were tested at a current density of 125 $mA \cdot cm^{-2}$, a B/C ratio of 4.9%, and a water flow rate of 36 $L \cdot h^{-1}$ (Figure 7).

As depicted in Figure 7, the ozone concentration and current efficiency increase accordingly as the electrode thickness is from 0.32 mm to 0.54 mm, this might be because that in the case of thinner electrodes, increasing electrode thickness enlarges the reaction interface, which contributes to the synthesis of ozone. However, as the electrode thickness exceeds 0.54 mm, the ozone concentration and current efficiency both begin to decrease. This might be because that a further increase in the electrode thickness increases the reaction resistance, leading to the increase of electric current that is used to overcome ohmic loss and then reducing the current efficiency. The maximum values of ozone concentration and current efficiency can be clearly observed at the BDD electrode with 0.54 mm in thickness and they are 35.46% and 5.88 $mg \cdot L^{-1}$, respectively.

Another very important observation in Figure 7(b) is that specific power consumption drops with electrode thickness rapidly down to a minimum value, and then increases. The drop of specific power consumption is due to that the increasing reaction interface increases O_3 formation rate and its raise is attributed to the elevation of cell voltage from 4.3 V at 0.32 mm in thickness to 7.43 V at 0.98 mm in thickness (shown in Figure 7(a)), which makes much power wasted in the production of heat. Under the trade-off relationship between higher EOP efficiency and higher cell voltage, a minimum specific power

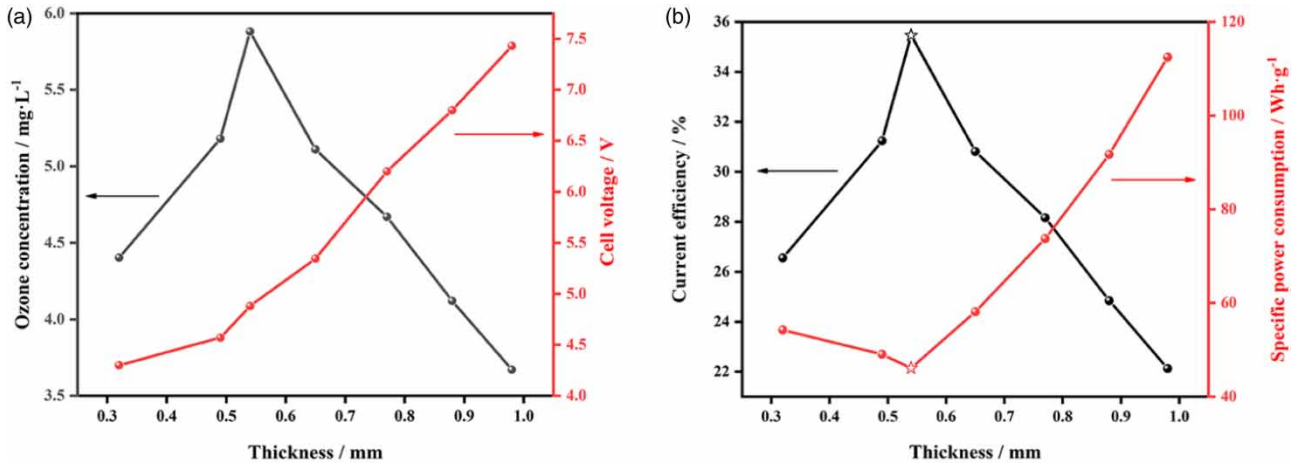

Figure 7 | The dependence of (a) ozone concentration and cell voltage, (b) current efficiency and specific power consumption on electrode thickness.

consumption of 46.11 Wh·g^{-1} is found to be around 0.54 mm. Those results demonstrate that a medium electrode thickness presents the superior EOP performance and the optimum electrode thickness is 0.54 mm.

The changes in EOP performance with water flow rate

Many previous studies have demonstrated that EOP performance is highly dependent on the water flow rate. To further elucidate this interesting point, the optimization of water flow rate was performed at a current density of 125 mA·cm^{-2}, a B/C ratio of 4.9%, and a thickness of 0.54 mm (Figure 8).

As illustrated in Figure 8, the current efficiency with the water flow rate increases up to a steady state value and then it is maintained. The current efficiency attains a maximum value of 51.29% at a water flow rate of 63 L·h^{-1}. The increase of current efficiency at a water flow rate below 63 L·h^{-1} is partly attributed to the employment of a flow system which builds a smooth way for the transfer of water to the electrode surface and the release of ozone from the electrode surface. Meanwhile, the higher water flow rate increases the ozone release rate, thus avoiding ozone destruction reactions. Another reason for the trend is that at lower water flow rate, the amount of ozone in the gas phase is promoted over that in the liquid phase, and increasing the flow rate is expected to effectively promote a change in this ratio (Onda *et al.* 2005). At a water flow rate over 63 L·h^{-1}, a stabilization in the current efficiency can be attributed to an equilibrium rate between the formation and destruction of ozone.

However, specific power consumption with the water flow rate decreases down to a steady state value and then it stays constant. A maximum value of 37.95 Wh·g^{-1} is achieved at a water flow rate of 63 L·h^{-1}. This is because the higher water flow rate allows rapid dispersion of the heat generated during electrolysis, thus minimizing ohmic loss. It can also be seen from Figure 8, the concentration of ozone water decreases as water flow rate is increased and it attains 4.86 mg·L^{-1} at the highest current efficiency and the lowest production energy.

Evaluation of the bactericidal effect of ozone water

After determining the optimal electrode configuration and operating conditions, 4.86 mg·L^{-1} of ozone water was produced by the SPE electrolyzer. To evaluate the bactericidal activity of ozone water, the death rate and growth reduction of E. coli with the inoculum concentrations ranged between 1×10^3 and 3×10^9 cfu·mL-1 were measured (Figure 9).

As the concentration of *E. coli* increases, the death rate and growth reduction both decrease. When the *E. coli* concentration is in the range of 1×10^3–3×10^3 cfu·mL-1, the death rate is 100% and the growth reduction is higher than 5 log. Under this condition the ozone water meets the disinfection standard and can be used as a disinfectant. When the *E. coli* with the inoculum concentrations of 1×10^9 to 3×10^9 cfu·mL-1 was exposed to ozone water for 10 min, the death rate and growth reduction were equal to 96.36% and 1.44 log, respectively. At this time the ozone water reaches the standard of bactericidal effect, demonstrating that the ozone water is also effective in inactivating the *E. coli* with high inoculum concentration. These results indicated that the ozone water shows a considerable bactericidal effect on different concentrations of *E. coli* and has great prospects for application in the environment field.

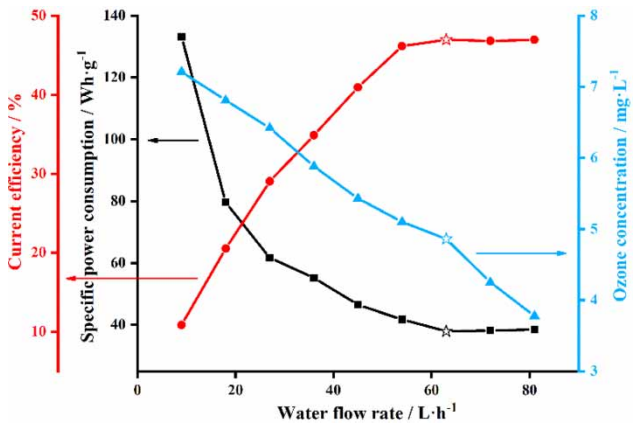

Figure 8 | The dependence of ozone concentration, current efficiency and specific power consumption on the water flow rate.

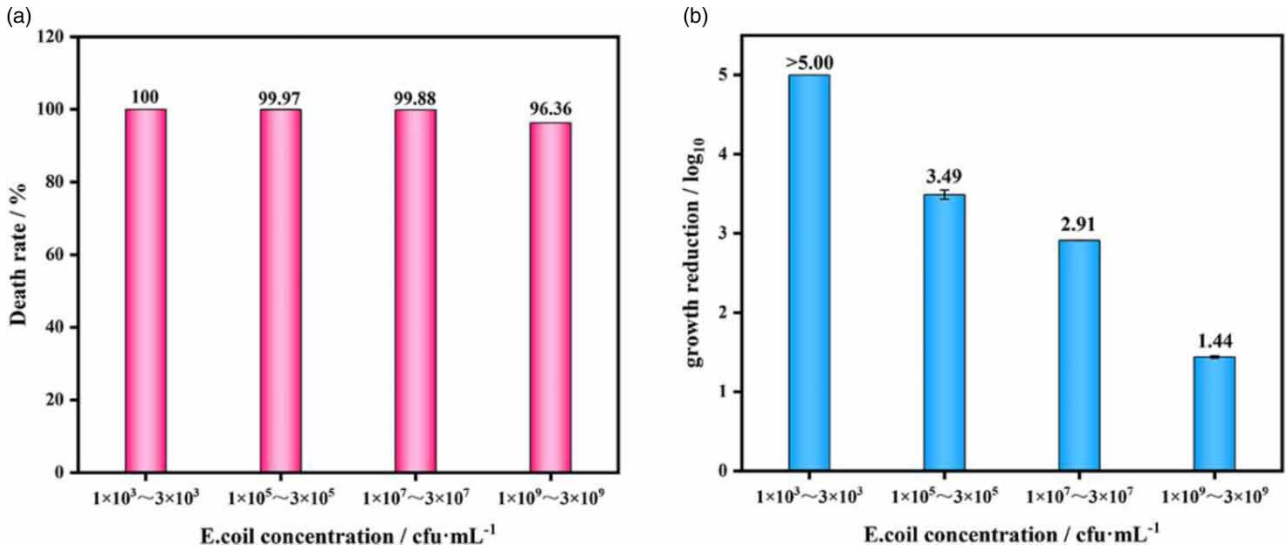

Figure 9 | Action of ozone water on the *E. coli* with different concentrations. Analysis of (a) the death rate and (b) growth reduction for the microorganism E. coli.

CONCLUSIONS

In summary, the SPE electrolyzer equipped with a couple of BDD electrodes was rationally designed and assembled, which can continuously and effectively produce ozone by a flow-through system with low energy consumption.

Electrode configuration studies revealed that the BDD electrode with a high B/C ratio (BDD-4.9) possess higher electrical conductivity and larger active surface area compared with the BDD electrode with a low B/C ratio, resulting in much improved ozone production efficiency, and the BDD electrode with 0.54 mm in thickness shows the superior EOP performance. The study concerning operating conditions indicated that ozone production is favored by the medium current density (125 $mA{\cdot}cm^{-2}$) and higher water flow rate (63 $L{\cdot}h^{-1}$).

The highest current efficiency of 51.29% and the lowest specific power consumption of 37.95 $Wh{\cdot}g^{-1}$ were achieved, which corresponds to an ozone concentration of 4.86 $mg{\cdot}L^{-1}$. This concentration of ozone water is effective in inactivating the E. coli with inoculum concentrations in the range of 1×10^3–3×10^9 $cfu{\cdot}mL^{-1}$. Application of the SPE electrolyzer for disinfection and sterilization will be expected in the future.

ACKNOWLEDGEMENTS

This work was supported by the National Natural Science Foundation of China (No. 51878659), Military Logistics Research (No. AWS18J004) and Youth Program of Military Medical Research Project of PLA General Hospital (QNF19051).

CONFLICTS OF INTEREST

The authors declare no conflict of interest.

DATA AVAILABILITY STATEMENT

All relevant data are included in the paper or its Supplementary Information.

REFERENCES

Arihara, K., Terashima, C. & Fujishima, A. 2007 Electrochemical production of high-concentration ozone-water using freestanding perforated diamond electrodes. *J. Electrochem. Soc.* **154** (4), 71–75.

Awad, M. I., Sata, S., Kaneda, K., Ikematsu, M. & Okajima, T. 2006a Ozone electrogeneration at a high current efficiency using a tantalum oxide-platinum composite electrode. *Electrochem. Commun.* **8** (8), 1263–1269.

Awad, M. I., Saleh, M. M. & Ohsaka, T. 2006b Ozone electrogeneration on Pt-loaded reticulated vitreous carbon using flooded and flow-through assembly. *J. Electrochem. Soc.* **153** (12), 207–212.

Azam, M., Restiwijaya, M., Zain, A., Sumariyah, S. & Nur, M. 2019 DDBD ozone plasma reactor generation: the proper dose for medical applications. *J. Phys.* **1217**, 012026.

Babak, A. A., Amadelli, R., Battisti, A. D. & Fateev, V. N. 1994 Influence of anions on oxygen/ozone evolution on PbO_2/SPE and PbO_2/Ti electrodes in neutral pH media. *Electrochim. Acta* **39** (11–12), 1597–1602.

Bogdanowicz, R., Ficek, M., Malinowska, N., Gupta, S., Meek, R., Niedziałkowski, P., Rycewicz, M., Sawczak, M., Ryl, J. & Ossowski, T. 2020 Electrochemical performance of thin free-standing boron-doped diamond nanosheet electrodes. *J. Electroanal. Chem.* **862**, 114016.

Coffinier, Y., Szunerits, S., Drobecq, H., Melnyk, O. & Boukherroub, R. 2011 Diamond nanowires for highly sensitive matrix-free mass spectrometry analysis of small molecules. *Nanoscale* **4** (1), 231–238.

Da Silva, L. M. D., Santana, M. H. P. & Boodts, J. F. C. 2003 Electrochemistry and green chemical processes: electrochemical ozone production. *Química Nova* **26** (6), 880–888.

Dettlaff, A., Sobaszek, M., Klimczuk, T. & Bogdanowicz, R. 2020 Enhanced electrochemical kinetics of highly-oriented (111)-textured boron-doped diamond electrodes induced by deuterium plasma chemistry. *Carbon* **174**, 594–604.

Ershov, B. G. & Morozov, P. A. 2008 Decomposition of ozone in water at pH 4–8. *Russ. J. Appl. Chem.* **81** (11), 1895–1898.

Foller, P. C. & Kelsall, G. H. 1993 Ozone generation via the electrolysis of fluoboric acid using glassy carbon anodes and air depolarized cathodes. *J. Appl. Electrochem.* **23** (10), 996–1010.

García-Espinoza, J. D., Robles, I., Durn-Moreno, A. & Godínez, L. 2021 Photo-assisted electrochemical advanced oxidation processes for the disinfection of aqueous solutions: a review. *Chemosphere* **274**, 129957.

Goztas, Z., Onat, H., Tosun, G., Sener, Y. & Hadimli, H. H. 2014 Antimicrobial effect of ozonated water, sodium hypochlorite and chlorhexidine gluconate in primary molar root canals. *Eur. J. Paediatric Dent.* **8** (4), 469–474.

Graça, A., Abadias, M., Salazar, M. & Nunes, C. 2011 The use of electrolyzed water as a disinfectant for minimally processed apples. *Postharvest Biol. Technol.* **61** (2–3), 172–177.

Gu, Y., Wang, S., Shi, H., Yang, J. & Wang, J. 2021 Atomic Pt embedded in BNC nanotubes for enhanced electrochemical ozone production via an oxygen intermediate-rich local environment. *ACS Catal.* **11** (9), 5438–5451.

Honda, Y., Ivandini, T. A., Watanabe, T., Murata, K. & Einaga, Y. 2013 An electrolyte-free system for ozone generation using heavily boron-doped diamond electrodes. *Diamond Relat. Mater.* **40**, 7–11.

Kraft, A., Stadelmann, M. & Wünsche, M. 2006 Electrochemical ozone production using diamond anodes and a solid polymer electrolyte. *Electrochem. Commun.* **8** (5), 883–886.

Lara-Ramos, J. A., Saez, C., Machuca-Martínez, F. & Mar, B. 2020 Electro-ozonizers: A new approach for an old problem. *Sep. Purif. Technol.* **241**, 116701.

Lees, C. M., Lansing, J. L. & Morelly, S. L. 2018 Ni- and Sb-doped SnO_2 electrocatalysts with high current efficiency for ozone production via electrodeposited nanostructures. *J. Electrochem. Soc.* **165** (16), 833–840.

Liu, C. L., Han, Y. H., Wang, Y., Peng, G., Wu, B. J. & Gao, C. X. 2011 Preparation and characterization of boron doped diamond electrodes on diamond anvil for in situ electrical measurements under high pressure. *Diamond Relat. Mater.* **20** (2), 250–253.

Michaud, P. A., Panizza, M. & Ouattara, L. 2003 Electrochemical oxidation of water on synthetic boron-doped diamond thin film anodes. *J. Appl. Electrochem.* **33** (2), 151–154.

Mortet, V. & Soltani, A. 2011 Impurity impact ionization avalanche in p-type diamond. *Appl. Phys. Lett.* **99** (20), 3.

Okino, F., Kawaguchi, Y., Touhara, H., Momota, K., Nishitani-Gamo, M., Ando, T., Sasaki, A., Yoshimoto, M. & Odawara, O. 2004 Preparation of boron-doped semiconducting diamond films using BF_3 and the electrochemical behavior of the semiconducting diamond electrodes. *J. Fluorine Chem.* **125** (11), 1715–1722.

Onda, K., Ohba, T., Kusunoki, H., Takezawa, S., Sunakawa, D. & Araki, T. 2005 Improving characteristics of ozone water production with multilayer electrodes and operating conditions in a polymer electrolyte water electrolysis cell. *J. Electrochem. Soc.* **152** (10), 177–183.

Rodríguez-Peña, M., Barrios Pérez, J. A., Llanos, J., Saez, C., Rodrigo, M. A. & Barrera-Díaz, C. E. 2021a New insights about the electrochemical production of ozone. *Curr. Opin. Electrochem.* **27**, 100697.

Rodríguez-Peña, M., Barrios Pérez, J. A., Llanos, J., Sáez, C., Barrera-Díaz, C. E. & Rodrigo, M. A. 2021b Electrochemical generation of ozone using a PEM electrolyzer at acidic pHs. *Sep. Purif. Technol.* **267**, 118672.

Rodríguez-Peña, M., Barrios Pérez, J. A., Llanos, J. & Rodrigo, M. A. 2021c Understanding ozone generation in electrochemical cells at mild pHs. *Electrochim. Acta* **376**, 138033.

Rosal, R., Rodríguez, A. & Perdigón-Melón, J. A. 2008 Removal of pharmaceuticals and kinetics of mineralization by O(3)/H(2)O(2) in a biotreated municipal wastewater. *Water Res.* **42** (14), 3719–3728.

Sandin, S., Hamad, A. A., Cuartero, M., Marco, R. D. & Cornell, A. 2020 Deactivation and selectivity for electrochemical ozone production at Ni- and Sb-doped SnO2/Ti electrodes. *Electrochim. Acta* **335**, 135645.

Santana, M. H. P., Faria, L. A. D. & Boodts, J. F. C. 2005 Electrochemical characterisation and oxygen evolution at a heavily boron doped diamond electrode. *Electrochim. Acta* **50** (10), 2017–2027.

Santos, L. M. C. D., Silva, E., Oliveira, F. O., Rodrigues, L. & Machado, B. 2021 Ozonized water in microbial control: analysis of the stability, in vitro biocidal potential, and cytotoxicity. *Biology* **10**, 525.

Silva, L. M. D., De Faria, L. A. & Boodts, J. F. C. 2001 Green processes for environmental application. Electrochemical ozone production. *Pure Appl. Chem.* **73** (12), 1871–1884.

Uhm, H. S., Lee, K. H. & Seong, B. L. 2009 Inactivation of H1N1 viruses exposed to acidic ozone water. *Appl. Phys. Lett.* **95** (17), 17.

Wang, J. P. & Jing, X. L. 2012 Study on the effect of the lead dioxide particles on the anodic electrode performance for ozone generation. *Electrochemistry* **74** (7), 539–543.

Wang, J. P., Xiang, X., Guo, L. H. & Luo, X. 2008 Effect of surface morphology of lead dioxide particles on their ozone generating performance. *Appl. Surf. Sci.* **254** (20), 6666–6670.

Zhang, C., Xu, Y., Lu, P., Zhang, X., Xu, F. & Shi, J. 2017 Capillary effect-enabled water electrolysis for enhanced electrochemical ozone production by using bulk porous electrode. *J. Am. Chem. Soc.* **139** (46), 16620–16629.

Zhang, K., Wang, H., Zhao, Y., Xi, Y. & Wang, Z. 2021 Preparation and electrochemical properties of boron-doped polycrystalline diamond film with five-fold twin structure. *Appl. Surf. Sci.* **568** (9), 150977.

Zhao, Y., Yu, H. T., Quan, X., Chen, S., Zhao, H. M. & Zhang, Y. B. 2014 Preparation and characterization of vertically columnar boron doped diamond array electrode. *Appl. Surf. Sci.* **303**, 419–424.

First received 25 November 2021; accepted in revised form 15 January 2022. Available online 28 January 2022